Surrogate Modeling Strategy for Random Fields with Uncertain Correlation Lengths

Emily Zeller, Maximilian Schweizer, Marc Fina, Werner Wagner and Steffen Freitag
Institute for Structural Analysis, Karlsruhe Institute of Technology, Karlsruhe 76131, Germany,
emily.zeller@kit.edu

Abstract. Thin-walled shell structures achieve high load-bearing capacities with low material consumption. However, they are highly susceptible to stability issues caused by geometric imperfections. To account for these imperfections, random fields are incorporated into finite element (FE) models, and the structural response is evaluated with Monte Carlo simulations. Time-consuming FE analyses can be replaced by an artificial neural network (ANN) surrogate model. When applying the Karhunen-Loève expansion (KLE), the shape of the random field is determined by a correlation length, which may be affected by epistemic uncertainty. Consequently, the random field is modeled using fuzzy correlation lengths, leading to a further increase in computation time. To reduce this effort, an interpolation-based surrogate modeling strategy is proposed and compared with the conventional approach of solving the KLE eigenvalue problem. Within a multilevel surrogate modeling framework, the ANN is combined with least-squares polynomials to perform a structural optimization including fuzzy stochastic analysis. The introduced model is then applied to a fiber composite plate to optimize its thickness and fiber orientation angle. Therefore, both single-objective constrained and multi-objective unconstrained optimization are conducted.

Keywords: multilevel surrogate modeling, fuzzy stochastic analysis, polymorphic uncertainty, uncertain correlation length, Karhunen-Loève expansion, artificial neural network, structural design optimization

1. Introduction

The design of structures commonly involves an optimization process aiming to achieve high load-bearing capacities with minimal material consumption. Consequently, thin-walled shell structures are widely employed. In practice, however, their behavior is strongly influenced by geometric imperfections (Donnell and Wan, 1950). Deviations from the perfect geometry increase the susceptibility to stability problems, which can lead to a significant reduction in load-bearing capacity. In finite element (FE) analyses, geometric imperfections are incorporated by applying correlated random fields (Yang et al., 2022).

One approach to generate random fields is the Karhunen-Loève expansion (KLE), in which the spatial characteristics of the imperfections are primarily determined by the so-called correlation length ℓ_c (Schenk and Schuëller, 2007; Lauterbach et al., 2018). To obtain a realistic model, the correlation length can be derived from measurements of real structures, see (Fina et al., 2020; Fina et al., 2023). Due to the limited amount of available data, the correlation length is affected by epistemic uncertainty. The performance of a fuzzy stochastic analysis (Schweizer et al., 2025b) allows the consideration of uncertainty within numerical simulations. However, the integrated Monte Carlo simulation (MCS) requires a large number of FE evaluations, entailing a substantial computational cost. This effort can be reduced by employing an artificial neural network (ANN) as a surrogate model for the FE buckling calculation, see (Schweizer et al., 2025a; Schweizer et al., 2025b). If the correlation length is treated as an uncertain input parameter, the eigenvalue problem of the KLE has to be solved separately for each correlation length, which increases the computation time for generating the ANN training data. Therefore, an interpolation-based strategy is introduced, replacing the conventional solution of the KLE eigenvalue problem.

In this contribution, the fuzzy stochastic analysis is combined with an optimization loop in order to design robust and high-performing shell structures with low material usage. Thus, an ANN surrogate model is developed in which the design variables for the optimization process are incorporated as additional input variables alongside the uncertain a priori parameters. Therefore, the ANN proposed in (Schweizer et al., 2025b) is extended to account for uncertain correlation lengths. Moreover, least-squares (LSQ) polynomials complement the ANN within a multilevel surrogate modeling approach. This computational framework is used for both single-objective constrained and multi-objective unconstrained optimization to determine the optimal structural design of a fiber composite plate.

2. Optimization of Geometrically Imperfect Structures under Polymorphic Uncertainty

Apart from theoretical considerations, real-world structures are commonly affected by several kinds of uncertainty. According to (Götz et al., 2015; Der Kiureghian and Ditlevsen, 2009), it can be distinguished between aleatory and epistemic uncertainty. While aleatory uncertainty describes inherent natural variability, epistemic uncertainty results from incomplete information and imprecisions. The combination of both types is referred to as polymorphic uncertainty, also known as mixed or hybrid uncertainty. In the following, this concept is incorporated into structural design optimization.

2.1. Modeling of Geometric Imperfections

Geometric imperfections are modeled by applying a correlated random field to the FE model of the investigated structure, representing deviations of the surface geometry in the normal direction. In this contribution, the random fields are generated using the KLE, which is briefly summarized based on (Sudret and Der Kiureghian, 2000), (Vanmarcke, 2010) and (Zhang and Ellingwood, 1994).

In general, a random field

$$w(\boldsymbol{x}, \theta) = \{X(\boldsymbol{x}, \theta) \mid \boldsymbol{x} \in \Omega, \theta \in \Theta\} \tag{1}$$

assigns a random variable to each spatial point $\boldsymbol{x}$ and each event θ, where Ω denotes the surface of the structure and Θ represents the set of all possible events. Within the KLE framework, the random field is discretized at the n FE nodes and the autocorrelation matrix

$$\boldsymbol{\rho} = \begin{bmatrix} \rho(\boldsymbol{x}_1, \boldsymbol{x}_1) & \cdots & \rho(\boldsymbol{x}_1, \boldsymbol{x}_n) \\ \vdots & \ddots & \vdots \\ \rho(\boldsymbol{x}_n, \boldsymbol{x}_1) & \cdots & \rho(\boldsymbol{x}_n, \boldsymbol{x}_n) \end{bmatrix} \tag{2}$$

is employed, which is symmetric and positive definite. For generating the random field, the eigenvalue problem of the KLE

$$\boldsymbol{\rho} \cdot \boldsymbol{\varphi} = \lambda \cdot \boldsymbol{\varphi} \tag{3}$$

has to be solved, where $\boldsymbol{\varphi}$ and λ denote the eigenvectors and eigenvalues, respectively. Thus, the discrete random field is defined by

$$\hat{w}(\boldsymbol{x}, \theta) = \sum_{i=1}^{n} \xi_i(\theta) \sqrt{\lambda_i}\, \varphi_i(\boldsymbol{x}) \tag{4}$$

with the standard normally distributed random variables $\xi_i(\theta) \sim \mathcal{N}(0, 1)$.

If the structure is discretized with a large number of FE nodes n, many terms are required to construct the series given in Eq. (4). Hence, it is reasonable to truncate the series by discarding terms associated with small eigenvalues, which, therefore, have a negligible influence on the resulting random field. This truncation is performed using the quality index Q

$$\sum_{i=1}^{\tilde{n}} \lambda_i \geq Q \cdot \sum_{i=1}^{n} \lambda_i \tag{5}$$

after sorting the eigenvalues in descending order, thereby reducing the number of retained terms from n to $\tilde{n}$. Following (Brenner, 1995), a quality index of $Q = 99\,\%$ is adopted.

The entries of the autocorrelation matrix $\boldsymbol{\rho}$, introduced in Eq. (2), are specified through the autocorrelation function. Here, the squared exponential function

$$\rho(\boldsymbol{x}_i, \boldsymbol{x}_j) = \exp\left[-\frac{d^2(\boldsymbol{x}_i, \boldsymbol{x}_j)}{\ell_c^2}\right] \tag{6}$$

is employed, depending on the distance between the FE nodes $d(\boldsymbol{x}_i, \boldsymbol{x}_j)$ and the correlation length ℓ_c.

By varying ℓ_c, the spatial characteristics of the random field can be controlled systematically. Large values of ℓ_c correspond to highly correlated, smooth fields, whereas small values lead to more irregular realizations. This relationship is illustrated in Figure 1, where three different correlation lengths are used to generate a random field based on the same set of random variables $\boldsymbol{\xi}$. The correlation length ℓ_c can be obtained from measurements of structural surfaces, as demonstrated in (Fina et al., 2023).

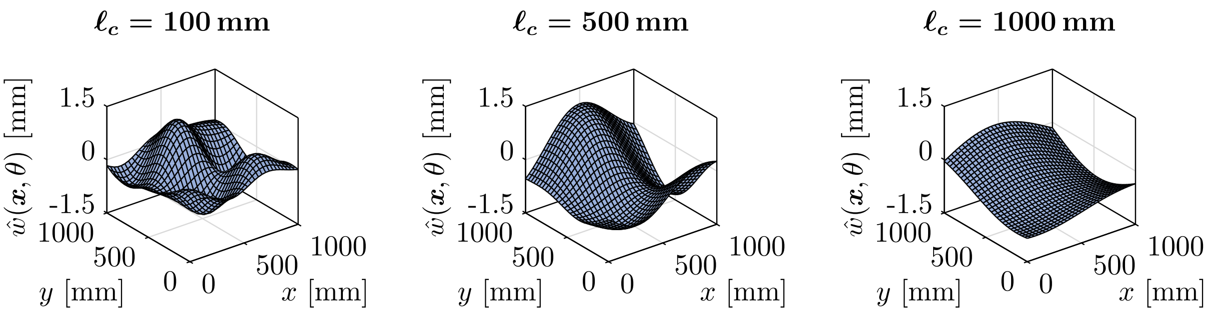

Figure 1. Influence of the correlation length on the random field of a square plate with the lateral dimension $L = 1000\,\mathrm{mm}$ and a discretization with $m = 30 \times 30 = 900$ elements

Since the available data are usually limited, ℓ_c is treated as an epistemically uncertain input parameter. The membership of the element ℓ_c to a set is rated gradually between $\mu(\ell_c) = 0$ and $\mu(\ell_c) = 1$ using the membership function $\mu(\ell_c)$. Consequently, the normalized fuzzy variable

$$\tilde{\ell}_c = \{(\ell_c, \mu(\ell_c)) \mid \ell_c \in \mathbb{R}\}, \quad \mu(\ell_c) : \mathbb{R} \to [0, 1] \tag{7}$$

can be introduced, see (Möller and Beer, 2004). If $\mu(\ell_c)$ is defined as a piecewise linear function that increases monotonically to its maximum $\mu(\ell_c) = 1$ and decreases monotonically thereafter, $\tilde{\ell}_c = \langle \ell_{c,1}, \ell_{c,2}, \ell_{c,3} \rangle$ is referred to as a convex fuzzy triangular variable, fully defined by its lower bound $\ell_{c,1}$, trend value $\ell_{c,2}$ and upper bound $\ell_{c,3}$.

By incorporating this fuzzy variable, Eq. (4) yields a so-called fuzzy probability-based random (fp-r) field, see (Schietzold et al., 2019). This field assigns an fp-r variable to each spatial point $\boldsymbol{x}$ and each event θ and is defined on the fuzzy probability space $(\Omega, \Sigma, \hat{P})$. The fuzzy probability $\hat{P} = (\hat{P}_\alpha)_{\alpha \in [0,1]}$ associates each α-level with an interval-valued probability measure

$$\hat{P}_\alpha = [\hat{P}^l_\alpha(\ell_c), \hat{P}^r_\alpha(\ell_c)], \quad 0 \leq \hat{P}^l_\alpha(\ell_c) \leq \hat{P}^r_\alpha(\ell_c) \leq 1 \quad . \tag{8}$$

2.2. Numerical Buckling Analysis

In this contribution, the load-bearing capacities of geometrically imperfect systems are investigated. Deviations from the reference geometry can limit the structural performance significantly. In general, slender structures subjected to compressive loading tend to fail due to stability phenomena. After the stability point is reached, large deformations occur, which are commonly referred to as buckling. In the following, a brief introduction to numerical buckling analysis is given based on (Wagner, 1995).

Reaching the stability point corresponds to an indifferent equilibrium state, which is numerically characterized by a singular tangential stiffness matrix $\boldsymbol{K}_T$. This critical point can be determined by performing either a linear or nonlinear buckling analysis. Linear buckling analysis neglects a possible nonlinear pre-buckling behavior, but, in those cases, provides sufficiently accurate results. This approach involves the decomposition of the tangential stiffness matrix

$$\boldsymbol{K}_T = \boldsymbol{K}_L + \boldsymbol{K}_{NL} \tag{9}$$

into the linear stiffness matrix $\boldsymbol{K}_L$ and the nonlinear stiffness matrix $\boldsymbol{K}_{NL}$. First, the linear solution at the origin of the load-displacement curve

$$\boldsymbol{K}_L \boldsymbol{u}_0 = \boldsymbol{P} \quad \Longleftrightarrow \quad \boldsymbol{u}_0 = \boldsymbol{K}_L^{-1} \boldsymbol{P} \tag{10}$$

is computed. Subsequently, the linear buckling analysis

$$[\boldsymbol{K}_L + \Lambda \boldsymbol{K}_{NL}(\boldsymbol{u}_0)]\boldsymbol{\varphi} = \boldsymbol{0} \tag{11}$$

can be performed, and the critical buckling load $\boldsymbol{P}_{\text{cr,perf}} = \Lambda \boldsymbol{P}$ as well as the associated critical displacement $\boldsymbol{u}_{\text{cr}} = \Lambda \boldsymbol{u}_0$ are obtained.

As a numerical example, an axially loaded composite plate is investigated. For this structure, the presence of geometric imperfections transforms the stability problem into a stress problem, since $\boldsymbol{K}_T$ no longer becomes singular. Therefore, no classical buckling analysis can be applied to determine the critical load. Following (Schweizer et al., 2025b), the critical load of the geometric imperfect structure is defined as the load corresponding to the critical displacement of the plate without imperfections, given by $P_{\text{cr}} = P(u_{\text{cr}})$. This concept is shown in Figure 2 for a square plate subjected to a distributed load p, resulting in a total load $P = p \cdot L$, where L denotes the lateral dimension.

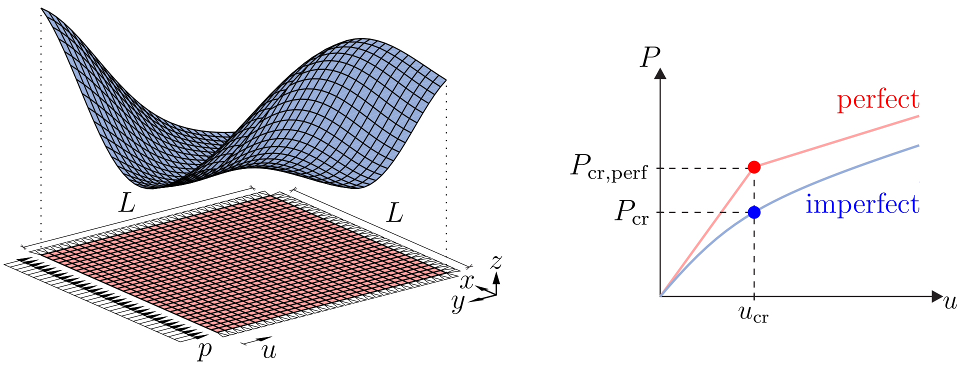

Figure 2. Influence of geometric imperfections on the load-displacement curve of an axially loaded plate

Moreover, geometric imperfections lead to a nonlinear response prior to reaching the critical displacement. A displacement-controlled arc-length method (Batoz and Dhatt, 1979; Wagner and Wriggers, 1988) is employed to generate the load-displacement curves and evaluate the critical load. To account for uncertain geometric imperfections, an MCS is performed, in which for each realization one random field is applied to the structure and the corresponding critical load P_{cr} is computed. Based on the MCS, an α-level optimization (Möller et al., 2000) is performed, in which the minimum and maximum stochastic responses are identified at discrete α-levels α_k. This procedure yields the fuzzy stochastic quantities of interest and the fuzzy cumulative distribution function (CDF) of the critical load P_{cr}. In this contribution, the mean value $E(P_{\text{cr}})$, the coefficient of variation $CV(P_{\text{cr}})$ and the 5% quantile $q_{0.05}(P_{\text{cr}})$ are evaluated. To render the fuzzy stochastic quantities suitable for the subsequent optimization, they have to be transformed into deterministic values by means of information reduction measures (Böttcher et al., 2023). As suggested in (Schweizer et al., 2025b), the centroids of these quantities are adopted (indicated by the index c).

2.3. Structural Design Optimization

Mathematically, an optimization problem is formulated as a minimization problem

$$\min[z(\boldsymbol{x}_d)], \quad \boldsymbol{x}_d \in \mathcal{D} \quad , \tag{12}$$

in which the objective function $z(\boldsymbol{x}_d)$ is minimized with respect to the design variables $\boldsymbol{x}_d$, see (Boyd and Vandenberghe, 2004). Both single-objective constrained and multi-objective unconstrained optimization are investigated and therefore introduced in the following.

In structural design, the aim is to achieve a high load-bearing capacity with a low dead load and, consequently, low material consumption by adjusting the design variables, e.g., thickness and fiber orientation. For structures with constant density, minimizing the dead load is equivalent to minimizing the volume. Accordingly, in the single-objective constrained approach, the volume is selected as the objective function $z(\boldsymbol{x}_d)$ to be minimized. To ensure sufficient load-bearing behavior, a threshold value P_{tr} is imposed. A high level of resistance is assessed by characterizing the load-bearing capacity through the 5% quantile of the critical load $q_{0.05,c}(P_{\mathrm{cr}}(\boldsymbol{x}_d))$. Thus, for constrained optimization, Eq. (12) is extended to

$$\min[z(\boldsymbol{x}_d)] \quad \text{subject to :} \quad q_{0.05,c}(P_{\mathrm{cr}}(\boldsymbol{x}_d)) \geq P_{\mathrm{tr}} \quad . \tag{13}$$

To account for this constraint, a modified objective function

$$\tilde{z}(\boldsymbol{x}_d) = z(\boldsymbol{x}_d) + \beta \cdot \underbrace{\max\{0,\, P_{\mathrm{tr}} - q_{0.05,c}(P_{\mathrm{cr}}(\boldsymbol{x}_d))\}}_{g(\boldsymbol{x}_d)} \tag{14}$$

is employed, incorporating the penalty function $g(\boldsymbol{x}_d)$ and the penalty factor β. Particle swarm optimization (PSO) is adopted as the numerical optimization algorithm, see, e.g., (Siarry, 2016).

Furthermore, a multi-objective unconstrained formulation is examined. To design a robust and high-performing system, two objective functions

$$z_1(\boldsymbol{x}_d) = CV_c(P_{\mathrm{cr}}(\boldsymbol{x}_d)), \quad z_2(\boldsymbol{x}_d) = -E_c(P_{\mathrm{cr}}(\boldsymbol{x}_d)) \tag{15}$$

are defined. The coefficient of variation $CV_c(P_{\mathrm{cr}}(\boldsymbol{x}_d))$ and the mean value $E_c(P_{\mathrm{cr}}(\boldsymbol{x}_d))$ represent robustness and performance, respectively. Since a large mean value is desirable, a negative sign is introduced to maintain the minimization framework. Moreover, a min-max normalization

$$z_i^*(\boldsymbol{x}_d) = \frac{z_i(\boldsymbol{x}_d) - z_{i,\min}}{z_{i,\max} - z_{i,\min}}, \quad 0 \leq z_i^*(\boldsymbol{x}_d) \leq 1, \quad i = 1, 2 \tag{16}$$

is applied to bring the objective functions onto comparable scales, using the minimum $z_{i,\min}$ and maximum $z_{i,\max}$ of each objective function within the design space, see (Miler et al., 2025). Analogously to the constrained approach, a PSO is employed. Because its standard formulation is restricted to single-criterion problems, the two normalized objectives are combined into a modified function based on Chebyshev scalarization

$$\tilde{z}(\boldsymbol{x}_d) = \max\{w_1 \cdot |z_1^*(\boldsymbol{x}_d)|;\; w_2 \cdot |z_2^*(\boldsymbol{x}_d)|\}, \quad 0 \leq w_1, w_2 \leq 1, \quad w_1 + w_2 = 1 \tag{17}$$

with weight factors w_1, w_2, see (Lin et al., 2024).

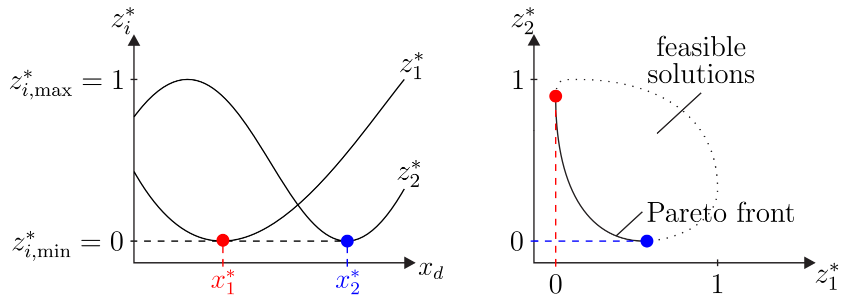

Figure 3. Determination of the Pareto front for two objective functions in a one-dimensional design space

In multi-objective optimization, a conflict of targets arises when the minima of the different objectives correspond to distinct design variable sets. In that case, no unique optimum exists. Instead, Pareto-optimal solutions can be identified, for which none of the objectives can be improved without deteriorating at least one of the others. These compromise solutions form the so-called Pareto front, as illustrated in Figure 3.

3. Computational Framework

The computational framework is divided into the fuzzy stochastic analysis and an structural optimization stage. First, the design variables $\boldsymbol{x}_d$ are introduced, which are subject to optimization. Within the design space, N_O uniformly distributed optimization sample points are selected. At each of these points, a fuzzy stochastic analysis is conducted. The correlation length is employed as a fuzzy triangular input variable $\tilde{\ell}_c = \langle \ell_{c,1}, \ell_{c,2}, \ell_{c,3} \rangle$ and is discretized into $N_\alpha = 11$ α-levels. At the lowest level $\mu(\ell_c) = 0$, N_F equidistant fuzzy sample points are defined. For each of them, an MCS is carried out to evaluate P_{cr} for N_{MCS} realizations with different geometric imperfections. In total, $N_O \times N_F \times N_{MCS}$ realizations are required.

To reduce the computational cost, an ANN is employed as a surrogate model $\hat{\mathcal{M}}_1(\ell_c, \boldsymbol{x}_d, \boldsymbol{\xi})$ for the time-consuming FE calculations. Based on (Schweizer et al., 2025a), the ANN is implemented as a feed-forward multilayer perceptron, comprising three hidden layers with ten neurons each. As proposed in (Schweizer et al., 2025b), the design variables $\boldsymbol{x}_d$ and the standard normally distributed random variables $\boldsymbol{\xi} = (\xi_1, \ldots, \xi_M)$ serve as input to the ANN. To incorporate fuzzy correlation lengths, the ANN input vector is extended by adding the correlation length ℓ_c.

The number M of the standard normally distributed random variables corresponds to the required terms of the KLE, which is reduced from n to $\tilde{n}$ by applying the quality index Q, given in Eq. (5). Since $\tilde{n}$ varies with ℓ_c, the maximum value $\tilde{n}_{\max}$, occurring for the smallest correlation length $\ell_{c,1}$, is determined in advance. Thus, $M = \tilde{n}_{\max}$ random variables are used as ANN inputs to maintain a constant network architecture. Consequently, for each correlation length $\tilde{n} = \tilde{n}_{\max}$ terms are retained when constructing the KLE.

For the following α-level optimization, an LSQ polynomial surrogate model $\hat{\mathcal{M}}_2(\ell_c)$ is employed. This procedure yields the fuzzy stochastic output, from which the corresponding centroids $E_c(P_{\text{cr}})$, $CV_c(P_{\text{cr}})$ and $q_{0.05,c}(P_{\text{cr}})$ are evaluated. The same process is repeated for all optimization sample points. Subsequently, additional LSQ polynomial surrogate models $\hat{\mathcal{M}}_3(\boldsymbol{x}_d)$ are constructed to represent the dependence of these quantities on the design variables. On this basis, the structural optimization is carried out and the optimal design within the admissible domain is determined. Figure 4 provides an overview of the adopted computational framework.

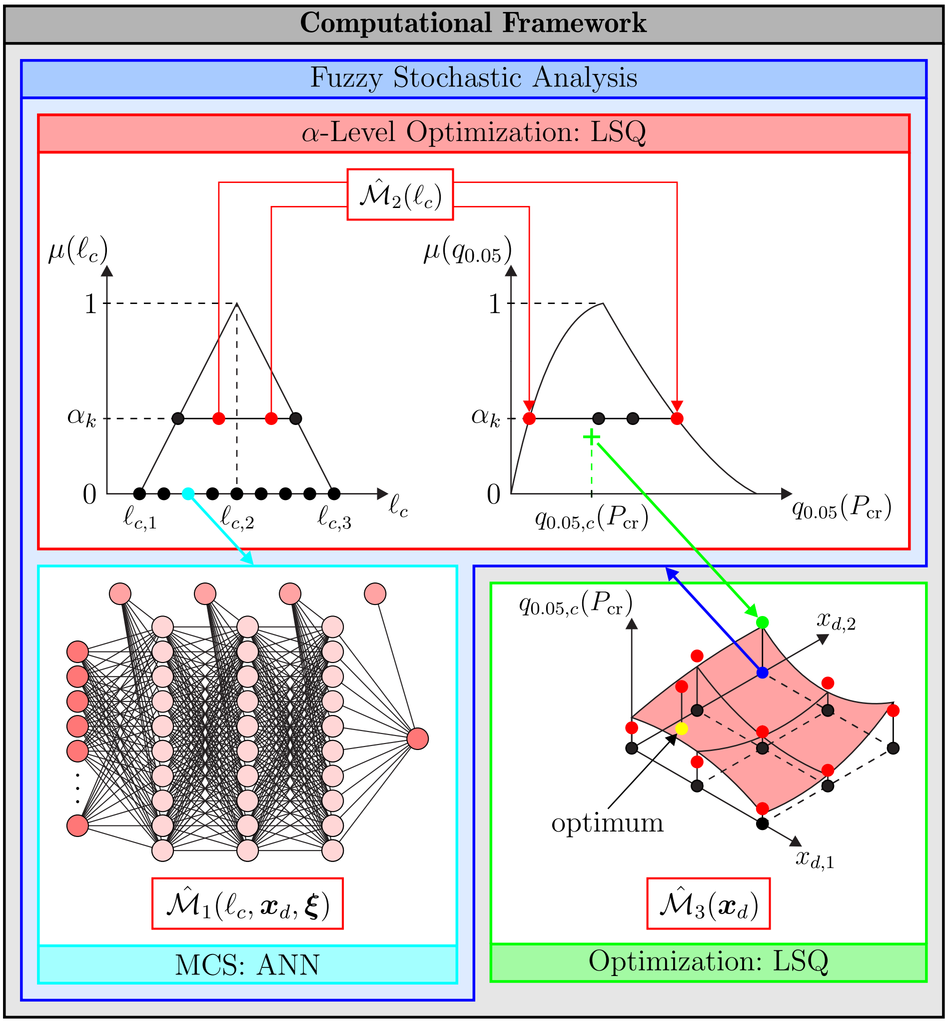

Figure 4. Procedure of the structural optimization including fuzzy stochastic analysis using three surrogate models for a two-dimensional design space, shown for the 5% quantile $q_{0.05}(P_{\mathrm{cr}})$

4. Numerical Example

The previously introduced framework is applied to a fiber composite plate that has been investigated in (Gürdal et al., 2008; Fina and Bisagni, 2025; Schweizer et al., 2025b). The plate has a lateral dimension of 1000 mm and is subjected to an axial load along the free edge with the resulting load $P = p \cdot 1000\,\text{mm}$. In the direction of thickness, the structure consists of twelve plies with different fiber orientation angles. A symmetric laminate configuration $[\pm\alpha]_{3s}$ is adopted, as illustrated in Figure 5. Moreover, transversely isotropic material behavior is assumed, and the corresponding properties are provided therein.

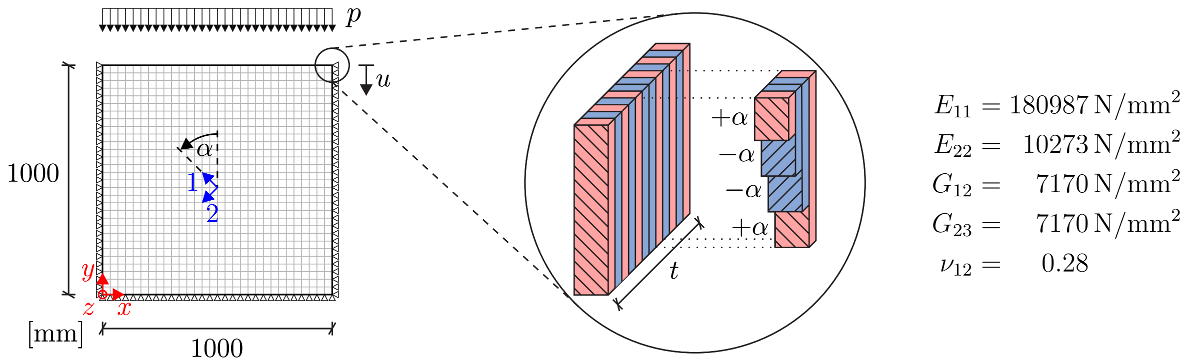

Figure 5. FE model and material properties of the investigated fiber composite plate

For FE calculations, the system is discretized with $m = 30 \times 30 = 900$ nonlinear four-node shell elements with moderate rotations and internal stacking (Wagner and Gruttmann, 1994; Wagner and Gruttmann, 2005; Gruttmann and Wagner, 2006), resulting in a total of $n = 961$ nodes. The correlation length is introduced as the fuzzy triangular variable $\tilde{\ell}_c = \langle 500, 750, 1000\rangle\,\text{mm}$, which leads to a truncation of the KLE from $n = 961$ to $\tilde{n}_{\max} = 13$ terms. The thickness $t = [1, 2]\,\text{mm}$ and the fiber orientation angle $\alpha = [0, 90]^\circ$ are selected as design variables. With respect to the adopted sampling scheme, $N_O \times N_F \times N_{MCS} = 361 \times 5 \times 10^4 = 1.8 \times 10^7$ realizations are required.

4.1. ANN Training and Testing

Due to the large number of realizations, employing an ANN as a surrogate model for the FE calculations is reasonable. The network is trained using $N_{\text{train}} = 10^4$ training samples, each characterized by a different correlation length as well as different design variables and random variables. A major challenge results from the fact that variations in ℓ_c lead to changes in both the eigenvalues λ and eigenvectors $\boldsymbol{\varphi}$. Consequently, the KLE eigenvalue problem from Eq. (3) has to be solved $N_{\text{train}} = 10^4$ times. For finely discretized models with n FE nodes, solving the eigenvalue problem of an $n \times n$ matrix corresponds to a high computation time. Therefore, an alternative strategy is developed to determine the eigenvalues and eigenvectors with respect to ℓ_c.

Numerically, the scaling factor of an eigenvector is not uniquely determined. While its magnitude is fixed by the applied solver, its sign is arbitrary. To ensure consistency of the eigenvectors corresponding to different correlation lengths, the smallest considered value $\ell_c = 500\,\text{mm}$ is chosen as a reference and all other eigenvectors are adjusted accordingly by enforcing a consistent sign convention. In addition, repeated eigenvalues require special treatment, since no fixed ordering of the associated eigenvectors is guaranteed. Therefore, the eigenpairs are sorted with respect to the reference eigenvectors. After sign-alignment and sorting, the eigenvectors of different correlation lengths exhibit only minor variations while preserving their overall spatial characteristics. Figure 6 presents the first eigenvector for several correlation lengths, both along the sequence of nodes and over the two-dimensional structural domain.

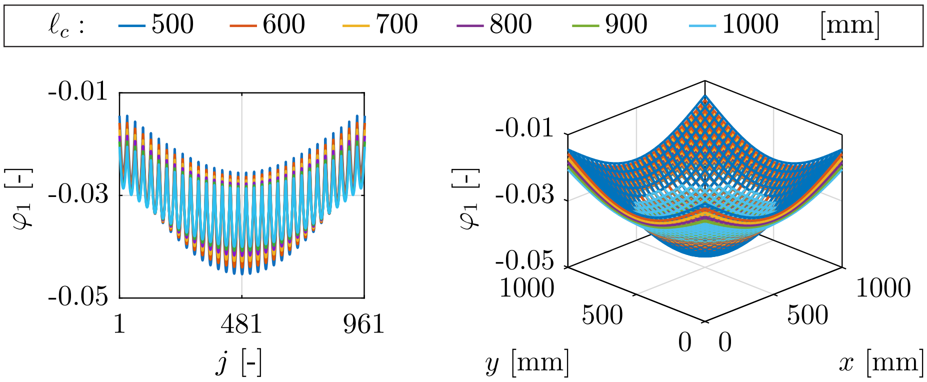

Figure 6. First eigenvector $\boldsymbol{\varphi}_1$ for $\ell_c = \{500, 600, \ldots, 1000\}$ mm, shown along the nodal index j and across the two-dimensional structure (x, y)

Motivated by this similar behavior, the eigenvector φ_i corresponding to an arbitrary value of ℓ_c is obtained by linear interpolation between the results for neighboring correlation lengths. The same procedure is applied to the eigenvalues λ. Thus, the eigenvalue problem of the KLE is solved once beforehand at discrete sampling points $\ell_c = \{500, 550, 600, \ldots, 1000\}$ mm instead of $N_{\text{train}} = 10^4$ times for each new ℓ_c during ANN training. In the following, this interpolation-based approach is denoted by *Int*, whereas the conventional solution of the KLE eigenvalue problem is referred to as *EVP*. The Int method is illustrated in Figure 7 for the first eigenvector of a one-dimensional structure and the complete set of eigenvalues.

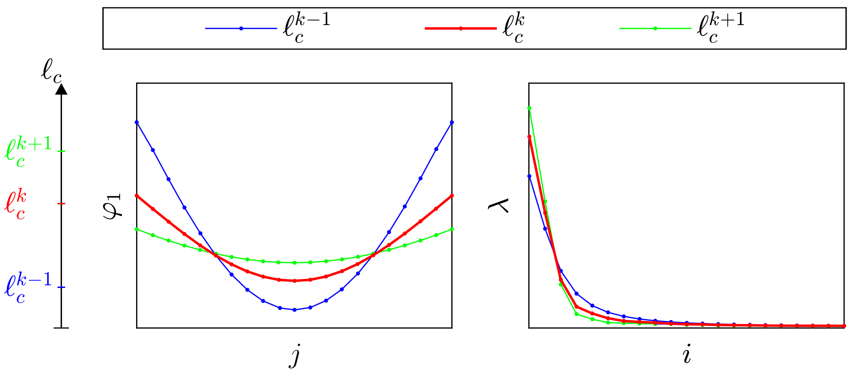

Figure 7. Scheme of the proposed interpolation-based method (Int) for a one-dimensional structure

To evaluate the efficiency of the proposed interpolation-based strategy, the ANN training is performed for different discretizations from $m = 10 \times 10 = 100$ to $m = 70 \times 70 = 4900$ elements and compared with the conventional solution of the eigenvalue problem. The 10^4 training samples are generated in a parallel loop with 12 processing cores operating at 4.70 GHz and 32 GB of

RAM under Windows 11. The resulting computation times for this environment are presented in Figure 8. For reference, the computation time of the EVP method using a discretization with $m = 100$ elements is normalized to 1, and all other efforts are expressed as a relative time factor.

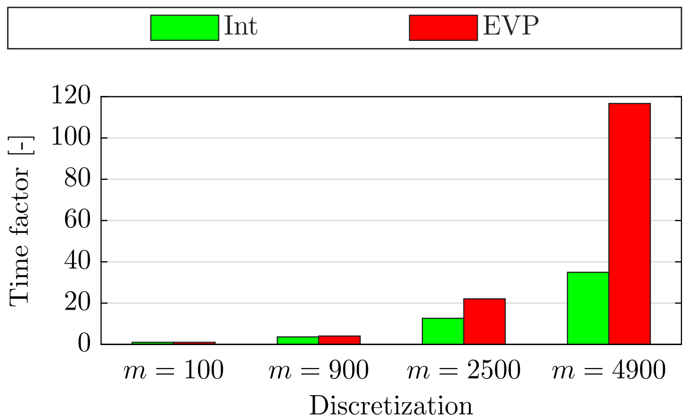

Figure 8. Normalized computation time to generate $N_{\text{train}} = 10^4$ training samples in a parallel loop using the Int and EVP methods for different discretizations with m elements

For coarse discretizations, the Int and EVP methods exhibit comparable computational costs. However, as the number of elements m increases, the Int approach becomes progressively more efficient than the EVP method. To assess the suitability of the interpolation-based strategy, ANN surrogate models are trained for both methods Int and EVP. The predictive accuracy of these neural networks is evaluated using regression diagrams. As shown in Figure 9, the ANN-predicted critical loads $P_{\text{cr,ANN}}$ exhibit only minor deviations from the corresponding FE results $P_{\text{cr,FE}}$.

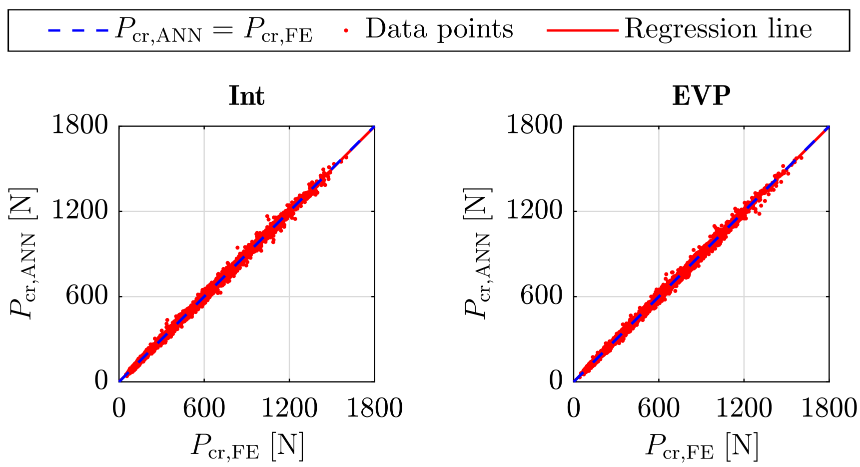

Figure 9. Regression diagrams of ANN training using the Int and EVP methods with $N_{\text{train}} = 10^4$

The high prediction quality is further confirmed through independent ANN plausibility testing. For this purpose, the correlation length is fixed at $\ell_c = 750\,\text{mm}$ and the random vector is set to

$\boldsymbol{\xi} = \mathbf{1}$. Moreover, one of the design variables is held constant at $t = 1.5\,\mathrm{mm}$ or $\alpha = 45\,°$, while the other design variable is varied equidistantly across the design space using $N_{\text{test}} = 19$ sampling points. In Figure 10, the resulting ANN predictions are compared with the FE solutions.

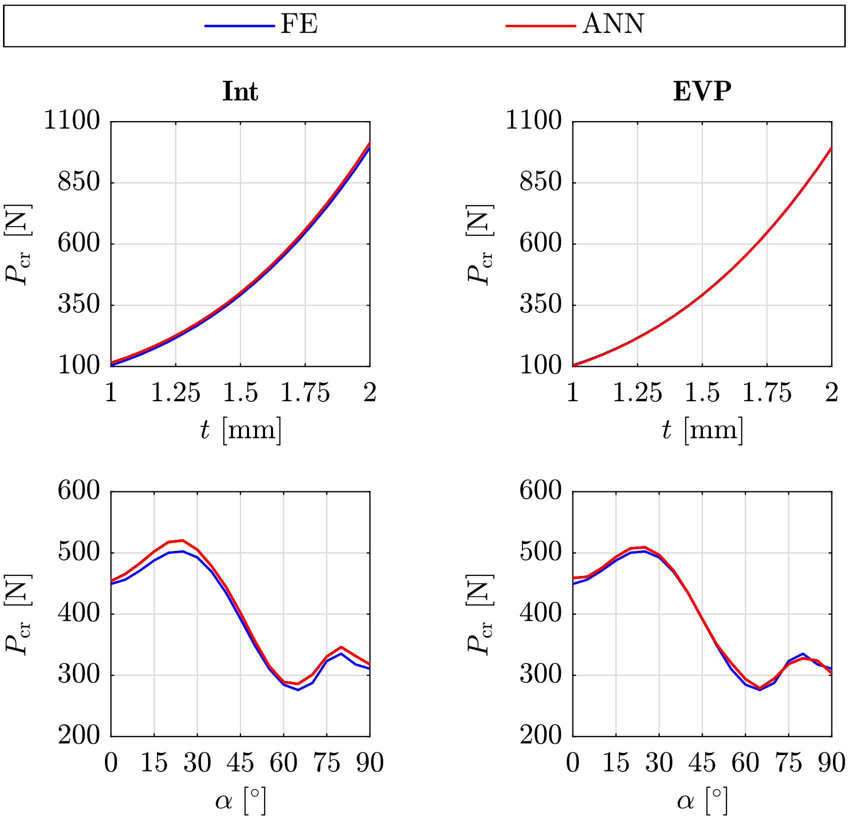

Figure 10. ANN testing using the Int and EVP methods for $t = [1, 2]\,\mathrm{mm}$ (top) and $\alpha = [0, 90]\,°$ (bottom) with $N_{\text{test}} = 19$

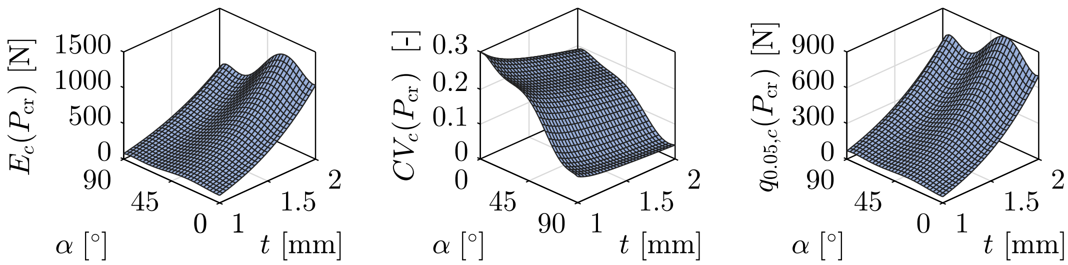

Figure 11. Predictions of the LSQ surrogate models for the mean value $E_c(P_{\text{cr}})$, coefficient of variation $CV_c(P_{\text{cr}})$ and 5% quantile $q_{0.05,c}(P_{\text{cr}})$ using the ANN EVP method with $N_O = 19 \times 19 = 361$

For both methods, the variation of P_{cr} with respect to the design variable is captured accurately by the neural networks. These results demonstrate that the ANN surrogate models are sufficiently reliable for the subsequent optimization studies. In the following, the two models are denoted by *ANN Int* and *ANN EVP* and used to construct separate LSQ surrogate models for the optimization stage. The results of the surrogate models generated by the ANN EVP method are presented in Figure 11.

4.2. Single-Objective Constrained Optimization

For the single-objective constrained optimization, the threshold value of the 5% quantile is prescribed as $P_{\text{tr}} = 500\,\text{N}$. To guarantee satisfaction of the constraint, a comparatively large penalty factor of $\beta = 10^4$ is adopted. Figure 12 illustrates the constraint of the 5% quantile $q_{0.05,c}(P_{\text{cr}})$ and the modified objective function $\tilde{z}$, see Eq. (14), over the design space, shown for the ANN EVP strategy. In addition, the corresponding optimum $(t_{\text{opt}}, \alpha_{\text{opt}})$ is indicated.

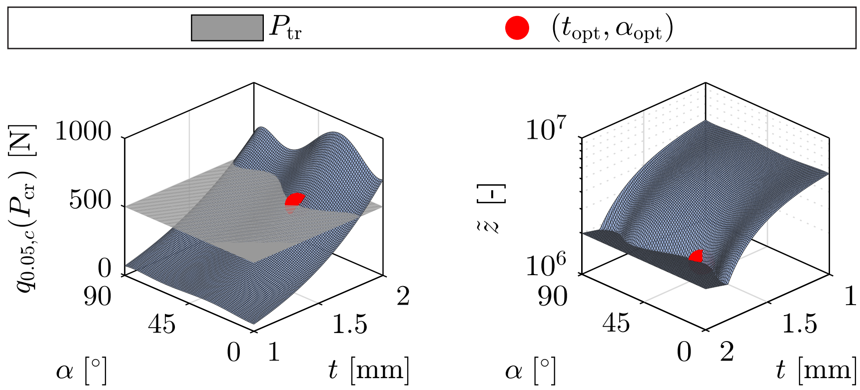

Figure 12. Determination of the optimum $(t_{\text{opt}}, \alpha_{\text{opt}})$ for the single-objective constrained optimization using the ANN EVP method, shown for the constraint $q_{0.05,c}(P_{\text{cr}})$ (left) and the modified objective function $\tilde{z}$ (right)

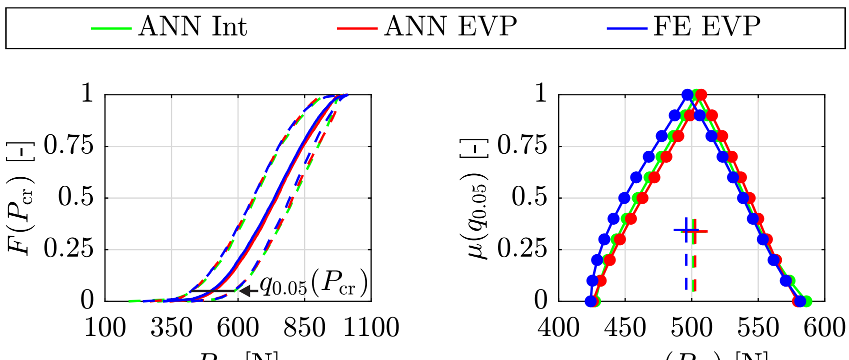

Figure 13. Fuzzy CDF and fuzzy 5% quantile $q_{0.05}(P_{\text{cr}})$ for the optimum $(1.68\,\text{mm}, 31.0\,°)$ of the single-objective constrained optimization using the ANN Int, ANN EVP and FE EVP methods with $N_{\text{MCS}} = 10^4$ and $N_F = 5$

Both methods identify similar optimal points $(1.685\,\text{mm}, 30.66\,°)$ and $(1.684\,\text{mm}, 31.21\,°)$. To derive the fuzzy stochastic output, the optimum is rounded to $(1.68\,\text{mm}, 31\,°)$. For validation purposes, a FE reference analysis is performed, in which the eigenvalue problem of the KLE is solved conventionally. The fuzzy CDF and the fuzzy 5% quantile of the critical load obtained with the methods ANN Int, ANN EVP and FE EVP are compared in Figure 13. To compute the fuzzy CDF, the probability $F(P_{\mathrm{cr}})$ is discretized with 100 quantile values. Overall, the close agreement among all approaches demonstrates the adequacy of the constructed ANN surrogate models in the constrained optimization setting.

4.3. Multi-Objective Unconstrained Optimization

According to the predictions of the surrogate models shown in Figure 11, the mean value of the critical load $E_c(P_{\mathrm{cr}})$ increases for larger thickness values t, whereas the coefficient of variation $CV_c(P_{\mathrm{cr}})$ decreases. Consequently, the multi-objective unconstrained optimum for maximizing $E_c(P_{\mathrm{cr}})$ and minimizing $CV_c(P_{\mathrm{cr}})$ is attained at the upper bound $t = 2\,\mathrm{mm}$, such that the optimization problem effectively reduces to one design variable α. The discrete weight factors of Chebyshev scaling in Eq. (17) are chosen as $w_1 = \{0, 0.05, 0.1, \dots, 1\}$ with $w_2 = 1 - w_1$. Figure 14 presents the resulting Pareto fronts generated using the ANN Int and ANN EVP approaches in both the normalized and original objective spaces. In addition, the optimal fiber orientation α_{opt} is shown with respect to the weight factor w_1.

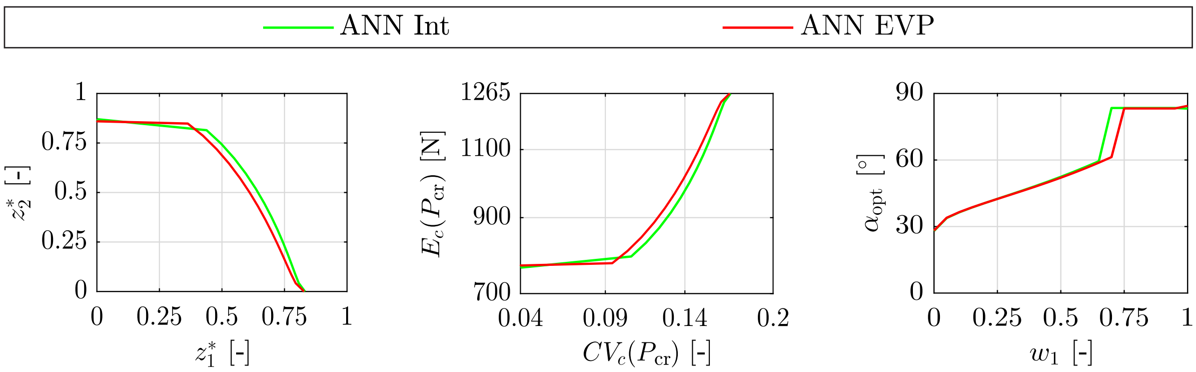

Figure 14. Results of the multi-objective unconstrained optimization using the ANN Int and ANN EVP methods: Pareto fronts in the normalized objective space (left) and original objective space (middle), and the corresponding optimum α_{opt} as a function of the weight factor w_1 (right)

Both methods produce closely matching results, confirming the suitability of the developed ANN surrogate models. With respect to the coefficient of variation, the minimum and, thus, the highest robustness are attained at $\alpha \approx 84\,°$, whereas the mean value reaches its maximum at $\alpha \approx 28\,°$, corresponding to the highest structural performance. In contrast to the single-objective constrained optimization with a unique optimum, a trade-off between robustness and performance is required to determine the final design. According to the individual preferences, the structural configuration can be selected from the set of Pareto-optimal solutions.

5. Conclusions

In this paper, a structural optimization framework incorporating fuzzy stochastic analysis was introduced. Therefore, random fields were generated within an MCS to represent aleatory uncertainty, while the correlation length of the KLE was treated as an epistemically uncertain input parameter. Structural optimization under polymorphic uncertainty substantially increases the computational effort because a large number of samples is required. Consequently, the use of efficient surrogate models becomes indispensable. Surrogate modeling was employed at three different stages. First, an ANN replaced FE calculations within the MCS. Moreover, an LSQ polynomial surrogate model was used for the α-level optimization and additional LSQ models were constructed to conduct the structural optimization within the design space.

Introducing the correlation length as a fuzzy variable further increases the computational cost, since the eigenvalue problem of the KLE has to be solved for each considered value of ℓ_c, which is particularly time-consuming for fine spatial discretizations. To mitigate this expense, an interpolation-based strategy was proposed and assessed against the conventional solution of the KLE eigenvalue problem. Separate neural networks were trained for both approaches and subsequently applied in two optimization settings. The single-objective constrained formulation targeted a reduction in structural mass while maintaining sufficient load-bearing capacity, resulting in a distinct optimum. In contrast, the multi-objective unconstrained formulation yielded a set of Pareto-optimal solutions, balancing structural performance and robustness.

Overall, both ANNs produced closely matching results. Thus, the proposed interpolation-based method constitutes an efficient alternative to repeatedly solving the eigenvalue problem of the KLE. In future studies, the correlation length could be derived from experimental surface measurements. The epistemic uncertainty caused by the limited amount of available data can be naturally incorporated into the developed computational framework. Additionally, alternative surrogate modeling techniques may be explored. For instance, convolutional neural networks can be used to predict the structural load-bearing capacity based on representations of geometric imperfections. Extending such approaches to account for epistemically uncertain correlation lengths that influence the spatial characteristics of the generated random fields represents a promising direction for further research.

References

Batoz, J.-L. and G. Dhatt: 1979, 'Incremental Displacement Algorithms for Nonlinear Problems'. *International Journal for Numerical Methods in Engineering* **14**(8), 1262–1267.

Böttcher, M., W. Graf, and M. Kaliske: 2023, 'Designing Structures with Polymorphic Uncertainty: Enhanced Decision Making Using Information Reduction Measures to Quantify Robustness'. *PAMM* **23**(4), e202300289.

Boyd, S. P. and L. Vandenberghe: 2004, *Convex Optimization.* Cambridge University Press.

Brenner, C.: 1995, 'Ein Beitrag Zur Zuverlässigkeitsanalyse von Strukturen Unter Berücksichtigung von Systemuntersuchungen Mit Hilfe Der Methode Der Stochastischen Finiten Elemente'. Ph.D. thesis, Fakultät für Bauingenieurwesen und Architektur, Universität Innsbruck.

Der Kiureghian, A. and O. Ditlevsen: 2009, 'Aleatory or Epistemic? Does It Matter?'. *Structural Safety* **31**(2), 105–112.

Donnell, L. H. and C. C. Wan: 1950, 'Effect of Imperfections on Buckling of Thin Cylinders and Columns Under Axial Compression'. *Journal of Applied Mechanics* **17**(1), 73–83.

Fina, M. and C. Bisagni: 2025, 'Buckling Design Optimization of Tow-Steered Composite Panels and Cylindrical Shells Considering Aleatory and Epistemic Uncertainties'. *Computational Mechanics* **76**(1), 59–92.

Fina, M., W. Wagner, and W. Graf: 2023, 'On Polymorphic Uncertainty Modeling in Shell Buckling'. *Computer-Aided Civil and Infrastructure Engineering* **38**(18), 2632–2647.

Fina, M., P. Weber, and W. Wagner: 2020, 'Polymorphic Uncertainty Modeling for the Simulation of Geometric Imperfections in Probabilistic Design of Cylindrical Shells'. *Structural Safety* **82**, 101894.

Götz, M., W. Graf, and M. Kaliske: 2015, 'Structural Design with Polymorphic Uncertainty Models'. *International Journal of Reliability and Safety* **9**(2/3), 112–131.

Gruttmann, F. and W. Wagner: 2006, 'Structural Analysis of Composite Laminates Using a Mixed Hybrid Shell Element'. *Computational Mechanics* **37**(6), 479–497.

Gürdal, Z., B. F. Tatting, and C. K. Wu: 2008, 'Variable Stiffness Composite Panels: Effects of Stiffness Variation on the in-Plane and Buckling Response'. *Composites Part A: Applied Science and Manufacturing* **39**(5), 911–922.

Lauterbach, S., M. Fina, and W. Wagner: 2018, 'Influence of Stochastic Geometric Imperfections on the Load-Carrying Behaviour of Thin-Walled Structures Using Constrained Random Fields'. *Computational Mechanics* **62**(5), 1107–1125.

Lin, X., X. Zhang, Z. Yang, F. Liu, Z. Wang, and Q. Zhang: 2024, 'Smooth Tchebycheff Scalarization for Multi-Objective Optimization'. *Proceedings of the 41th International Conference on Machine Learning*.

Miler, D., M. Hoić, R. Tomić, A. Jokić, and R. Mašović: 2025, 'Simultaneous Multi-Objective and Topology Optimization: Effect of Mesh Refinement and Number of Iterations on Computational Cost'. *Computation* **13**(7), 168.

Möller, B. and M. Beer: 2004, *Fuzzy Randomness*. Berlin, Heidelberg: Springer.

Möller, B., W. Graf, and M. Beer: 2000, 'Fuzzy Structural Analysis Using α-Level Optimization'. *Computational Mechanics* **26**(6), 547–565.

Schenk, C. A. and G. I. Schuëller: 2007, 'Buckling Analysis of Cylindrical Shells with Cutouts Including Random Boundary and Geometric Imperfections'. *Computer Methods in Applied Mechanics and Engineering* **196**(35), 3424–3434.

Schietzold, F. N., A. Schmidt, M. M. Dannert, A. Fau, R. M. N. Fleury, W. Graf, M. Kaliske, C. Könke, T. Lahmer, and U. Nackenhorst: 2019, 'Development of Fuzzy Probability Based Random Fields for the Numerical Structural Design'. *GAMM-Mitteilungen* **42**(1), e201900004.

Schweizer, M., M. Fina, W. Wagner, and S. Freitag: 2025a, 'Artificial Neural Networks for Random Fields to Predict the Buckling Load of Geometrically Imperfect Structures'. *Computational Mechanics* **76**(1), 181–204.

Schweizer, M., M. Fina, W. Wagner, and S. Freitag: 2025b, 'Optimization of Shell Structures with Fuzzy Probability-Based Random Fields Using Artificial Neural Networks'. *PAMM* **25**(4), e70038.

Siarry, P. (ed.): 2016, *Metaheuristics*. Cham: Springer International Publishing.

Sudret, B. and A. Der Kiureghian: 2000, *Stochastic Finite Element Methods and Reliability: A State-of-the-Art Report*. Departement of Civil & Environmental Engineering, University of California, Berkeley.

Vanmarcke, E.: 2010, *Random Fields: Analysis and Synthesis*. Singapore: World Scientific Publishing Co. Pte. Ltd., revised and expanded new edition.

Wagner, W.: 1995, 'A Note on FEM Buckling Analysis'. *Communications in Numerical Methods in Engineering* **11**(2), 149–158.

Wagner, W. and F. Gruttmann: 1994, 'A Simple Finite Rotation Formulation for Composite Shell Elements'. *Engineering Computations* **11**(2), 145–176.

Wagner, W. and F. Gruttmann: 2005, 'A Robust Non-Linear Mixed Hybrid Quadrilateral Shell Element'. *International Journal for Numerical Methods in Engineering* **64**(5), 635–666.

Wagner, W. and P. Wriggers: 1988, 'A Simple Method for the Calculation of Postcritical Branches'. *Engineering Computations* **5**(2), 103–109.

Yang, H., S. Feng, P. Hao, X. Ma, B. Wang, W. Xu, and Q. Gao: 2022, 'Uncertainty Quantification for Initial Geometric Imperfections of Cylindrical Shells: A Novel Bi-Stage Random Field Parameter Estimation Method'. *Aerospace Science and Technology* **124**, 107554.

Zhang, J. and B. Ellingwood: 1994, 'Orthogonal Series Expansions of Random Fields in Reliability Analysis'. *Journal of Engineering Mechanics* **120**(12), 2660–2677.